Available online at www.sciencedirect.com
SCIENCE DIRECT
Thermochimica Acta 446 (2006) 147–155
thermochimica acta
www.elsevier.com/locate/tca

Stochastic temperature modulation: A new technique in temperature-modulated DSC

J.E.K. Schawe [a,*], T. Hütter [a], C. Heitz [b], I. Alig [c], D. Lellinger [c]

[a] *Mettler-Toledo GmbH, Sonnenbergstrasse 74, CH-8603 Schwerzenbach, Switzerland*
[b] *Zurich University of Applied Science, P.O. Box 805, CH-8401 Winterthur, Switzerland*
[c] *Deutsches Kunststoff-Institut, Schlossgartenstrasse 6, D-64289 Darmstadt, Germany*

Received 22 December 2005; received in revised form 27 January 2006; accepted 29 January 2006
Available online 6 March 2006

Abstract

A new temperature-modulated differential scanning calorimetry (TMDSC) technique is introduced. The technique is based on stochastic temperature modulation and has been developed as a consequence of a generalized theory of a temperature-modulated DSC. The quasi-static heat capacity and the frequency-dependent complex heat capacity can be determined over a wide frequency range in one single measurement without further calibration. Furthermore, the reversing and non-reversing heat flows are determined directly from the measured data. Examples show the frequency dependence of the glass transition, the isothermal curing of thermosets and a solid–solid transition.

Keywords: Temperature-modulated DSC; Stochastic temperature modulation; Heat capacity; TOPEM®

1. Introduction

The heat flow Φ into the sample is usually described as the sum of two components, sensible and latent heat flow:

$$\Phi(T,t) = mc_p\beta + m\Delta h_r \frac{d\alpha}{dt} \quad (1)$$

where m is the sample mass, c_p the specific heat capacity, β the heating rate of the sample, Δh_r the specific enthalpy of a thermal event (e.g. enthalpy of reaction) and α is the extent of reaction (or more in general extent of structural change). In this paper the term heating rate is used in the sense of temperature change rate. This means in the case of cooling the heating rate is negative. The first term in Eq. (1) depends directly on the heating rate. This is the so-called sensible heat flow, Φ_{sens}. The latent heat flow, Φ_{lat}, is the second term in Eq. (1). It is determined by the physico-chemical processes in the sample, which are dependent on the change of internal variables far from an equilibrium state. Thus, Φ_{lat} is not primarily driven by the heating rate.

A conventional differential scanning calorimetry (DSC) experiment at a constant heating rate is not able to separate the two heat flow components of the measured signal. Various techniques of temperature-modulated DSC (TMDSC) have been developed to separate the heat flow components. In contrast to conventional DSC, the heating rate of a TMDSC measurement changes continuously. Typical examples of temperature programs are sequences of small temperature steps with isothermal segments [1] or a superimposition of a constant underlying heating rate β_u with a small periodic (e.g. sinusoidal) temperature perturbation [2]. Using such temperature modulation methods the change of the heat capacity during thermal events can be measured, even if the effect is masked by large quantities of latent heat (e.g. heat of reaction) or during quasi-isothermal measurements. Examples of such changes are the decrease of the heat capacity during the cold crystallization of amorphous materials [3], the decrease of c_p due to vitrification during polymerization [4–6] and the overlapping of the heat capacity change during the evaporation of volatiles [7,8].

A further aspect of TMDSC is the analysis of relaxation processes by measuring the frequency dependence of thermal events. For these measurements, the thermal response of the sample has to be analyzed at different frequencies. The simplest kind of a thermal relaxation is the thermal lag due to heat

* Corresponding author. Tel.: +41 1 806 7438; fax: +41 1 806 7240.
E-mail address: Juergen.schawe@mt.com (J.E.K. Schawe).

0040-6031/$ – see front matter © 2006 Elsevier B.V. All rights reserved.
doi:10.1016/j.tca.2006.01.031

transfer in the instrument and the sample. The result is that the heat capacity apparently becomes frequency dependent and a phase shift between heating rate and heat flow occurs. The information gained from the data can be used for the calibration of the TMDSC signals [9,10].

In addition to simple relaxations due to heat transport, the sample can show thermal relaxation processes due to the lag in heat transfer from the fast external to slow internal degrees of freedom. An example of such thermal relaxation processes is the entropy fluctuation due to the co-operative rearrangements in glass formers. This results in the heat capacity becoming time or frequency dependent. An example for such a relaxation process is the glass transition [11–14]. Analogous to the dielectric permittivity or the mechanical compliance the frequency-dependent heat capacity can be described by a complex function:

$$c_p^*(T,\omega) = c_\mathrm{f}(T) + c_\mathrm{s}^*(T,\omega) = c_\mathrm{f}(T) + c_\mathrm{s}'(T,\omega) - \mathrm{j}c_\mathrm{s}''(T,\omega) \tag{2}$$

where c_f is the part of the heat capacity due to the fast internal degrees of freedom. These are primarily vibrational modes. c_s is due to the slow internal degrees of freedom, which cause the frequency dependence of the heat capacity. This contribution of the heat capacity is related to all types of structural relaxations that occur close to (meta-stable) equilibrium. Because of the phase shift between heating rate and heat flow, the frequency-dependent heat capacity is a complex function containing a real part, c_s', and an imaginary part, c_s''. j is the imaginary unit. The knowledge gained through the frequency-dependent heat capacity provides information about the dynamics of the underlying molecular processes [14–16].

Depending on the focus of interest, two different evaluation approaches can be applied to TMDSC measurements. These are the determination of the frequency dependence of the complex heat capacity and the separation of the heat flow into two components. These components should be the sensible and latent heat flow. However, depending on the experimental conditions, the data determined can show significant deviations from these two heat flow components. The separated heat flow components are therefore named reversing and non-reversing heat flow. Different kinds of temperature modulation functions and evaluation procedures have been proposed:

(i) Stepwise temperature changes with isothermal segments [1,17–19]: these types of temperature programs are especially useful for the separation of the heat flow regarding Eq. (1). However, the time required for such experiments is relatively long because the sample should always relax to the equilibrium state during the isothermal segments.
(ii) Single frequency modulations: the modulation function can be sinusoidal [2,4,20,21] or more complex, for example a saw-tooth modulation [19,22]. Usually the first harmonic is used for evaluation procedures. The single-frequency modulation is used for the measurement of the frequency dependence of the heat capacity [20,23] or for separating the reversing and non-reversing heat flow components [2,21]. As discussed below, the disadvantage of this separation method is that the reversing and non-reversing heat flow generally does not match directly with the components in Eq. (1).
(iii) Multi-frequency periodic modulations generated by superposition of multiple sinusoidal functions [24] or the use of non-sinusoidal modulation functions evaluated by use of the Fourier transformation to get the spectral information [25]: these methods are used for calibration purposes or to measure the thermal relaxation of the sample.

A new advanced technique of temperature-modulated DSC should ideally combine the separation of sensible and latent heat flow and the measurement of the frequency-dependent heat capacity over a wide frequency range. The reversing and non-reversing heat flow components (Φ_rev and Φ_non) as determined by the evaluation procedure using single-frequency conventional TMDSC [26] cannot be directly discussed in terms of thermodynamic properties. The reason is the frequency dependence of the non-reversing heat flow. This problem is discussed in reference [27].

The demands for advanced TMDSC technologies can be summarized as follows:

(i) The measurement of the quasi-static heat capacity ($c_{p,0} = c_p^*(\omega \to 0) = c_p(t \to \infty)$).
(ii) The frequency independent determination of the non-reversing heat flow.
(iii) The ability to separate latent and sensible heat flow contributions.
(iv) The simultaneous determination of the frequency dependence of the heat capacity over a broad frequency range.

These requirements can be fulfilled in one single measurement by using stochastic temperature modulation [28]. The first results presented here show examples of a glass transition, a polymerization reaction and a second order phase transition.

2. Generalized theory of TMDSC

With the temperature programs commonly used for temperature modulation, the temperature given by the constant underlying heating rate β_u is superimposed by a small temperature perturbation $\delta T(t)$

$$\delta T(t) = \delta T_0 f_\mathrm{mod}(t) \tag{3}$$

where δT_0 is the maximum temperature perturbation (the amplitude for periodical modulation) and f_mod is the modulation function (for sinusoidal modulation $f_\mathrm{mod} = \sin(\omega_0 t)$; ω_0 is the used angular frequency). The modulated heating rate, $\beta_\mathrm{mod}(t)$ is the time derivative of Eq. (3). The Fourier transforms of $\delta T(t)$ and $\beta_\mathrm{mod}(t)$ are $\delta T(\omega)$ and $\beta_\mathrm{mod}(\omega) = \mathrm{j}\omega\delta T(\omega)$, respectively. In the time domain the total heating rate is:

$$\beta(t) = \beta_\mathrm{u} + \frac{\mathrm{d}}{\mathrm{d}t}(\delta T(t)) = \beta_\mathrm{u} + \beta_\mathrm{mod}(t) \tag{4}$$

and in the frequency domain:

$$\beta(\omega) = \beta_u \delta(\omega) + \beta_{mod}(\omega) \quad (5)$$

where ω is the angular frequency ($\omega = 2\pi f$; f is the frequency) and $\delta(\omega)$is the Dirac function. Combining Eqs. (1), (2) and (5) gives the heat flow in the frequency domain

$$\Phi(\omega) = mc_p^*(\omega)\beta(\omega) + m\Delta h_r j\omega\alpha \quad (6)$$

Eq. (6) is valid for measurements in which the sample shows linear behavior for the sensible heat flow component. The temperature perturbation δT due to the modulation must therefore be sufficiently small. For linear conditions, the heat capacity determined is invariant to δT change [29,30].

The relation between the frequency-dependent heat capacity and the time dependent heat capacity is given by [13]:

$$c_p^*(\omega) = c_f + \int_0^\infty \dot{c}_s(t)\, e^{-j\omega t}\, dt \quad (7a)$$

$$\dot{c}_s(t) = \frac{1}{2\pi}\int_{-\infty}^{\infty} (c_p^*(\omega) - c_f)\, e^{j\omega t}\, dt \quad (7b)$$

The inverse Fourier transformation of Eq. (6) yields the heat flow in the time domain. This transforms the simple algebraic product in the first term of Eq. (6) to a convolution product.

$$\Phi(t) = m(c_f\delta(t) + \dot{c}_s(t)) \otimes \beta(t) + m\Delta h_r\dot{\alpha} \quad (8)$$

where the convolution product is defined by $A(t) \otimes B(t) = \int_0^\infty A(t')B(t-t')\, dt'$. Thus, the first term in Eq. (8) is:

$$(c_f\delta(t) + \dot{c}_s(t)) \otimes \beta(t) = c_f\beta(t) + \int_0^\infty \dot{c}_s(t')\beta(t-t')\, dt' \quad (9)$$

According to Eq. (4) the heating rate is the sum of the constant underlying rate β_u and the rate due to the small temperature perturbation δT.

Eq. (8) describes the heat flow into an (infinitely thin) sample. The measured heat flow, Φ_m is to a good approximation a linear function of Φ. The reason for the difference between Φ and Φ_m is that the heat transfer conditions in the sample, crucible, and DSC sensor influence the signal shape. This results in a broadening of the heat flow peaks or steps. This effect is called smearing of the DSC curve by heat transfer. A simple model to describe such a smearing effect is given in reference [1]. If the DSC shows linear behavior, the smearing can be described by the linear response theory using a convolution integral [31,32]. The measured heat flow $\Phi_m(t)$ is then

$$\Phi_m(t) = \int_0^\infty G_s(t')\Phi(t-t')\, dt' = G_s(t) \otimes \Phi(t) \quad (10)$$

where G_s is the Green's function or impulse response function which describes all dynamic heat transfer influences in the sample and instrument from the measured curves (smearing). This means G_s characterizes the relation between the true heat flow into the infinitely thin sample and the measured curve. The integral of $G_s(t)$ is unity.

From Eqs. (8)–(10) the measured heat flow can be described as:

$$\Phi_m(t) = [G_s(t) \otimes m(c_f\delta(t) + \dot{c}_s(t))] \otimes \beta_m(t) + [G_s(t) \otimes m\Delta h_r\dot{\alpha}] \quad (11)$$

where β_m is the heating rate at the temperature sensor. If the dynamics of the latent heat flow is low compared to the time constant of the DSC, we can assume that this component is not smeared. With TMDSC measurements this is usually fulfilled because of the relative low underlying heating rate. Eq. (11) can then be simplified:

$$\Phi_m(t) = [G_s(t) \otimes m(c_f\delta(t) + \dot{c}_s(t))] \otimes \beta_m(t) + m\Delta h_r\dot{\alpha} \quad (12a)$$

or in the frequency domain

$$\Phi_m(\omega) = [g_s^*(\omega)mc_p^*(\omega)]\beta_m(\omega) + m\Delta h_r j\omega\alpha \quad (12b)$$

where $g_s^*(\omega)$ is the Fourier transform of $G_s(t)$.

$$g_s^*(\omega) = \int_0^\infty G_s(t)\, e^{-j\omega t}\, dt \quad (13)$$

The influence of the heat transfer and the heat capacity of the sample on the sensible heat flow component can be combined in the generalized impulse response function $G(t)$:

$$G(t) = G_s(t) \otimes m(c_f\delta(t) + \dot{c}_s(t)) \quad (14)$$

The measured heat flow is then the convolution product of the generalized impulse response function with the heating rate and the latent heat flow:

$$\Phi_m(t) = G(t) \otimes \beta_m(t) + m\Delta h_r\dot{\alpha} \quad (15a)$$

Fourier transformation of Eq. (15a) gives the frequency dependency of the measured heat flow

$$\Phi_m(\omega) = g^*(\omega)\beta_m(\omega) + m\Delta h_r j\omega\alpha \quad (15b)$$

where $g^*(\omega)$ is the Fourier transformed function of $G(t)$

$$g^*(\omega) = g_s^*(\omega)mc_p^*(\omega) \quad (16)$$

The experimental task is now to determine the latent heat flow and the function $g^*(\omega)$ using Eq. (15) within a frequency range that is as broad as possible. This problem can be solved if the heat flow signal has spectral contributions over a wide frequency range. A signal that fulfils this requirement is a suitably designed stochastic temperature perturbation (see below). $g^*(\omega)$ can then be determined by analyzing the correlation between the measured heat flow and the heating rate. According to Eq. (16) we understand $g^*(\omega)$ as a non-calibrated apparent complex heat capacity. The related complex calibration function for the determination of $mc_p^*(\omega)$ from $g^*(\omega)$ is then $1/g_s^*(\omega)$.

The quasi static heat capacity $c_{p,0}$ can be obtained through integration of $G(t)$ using Eq. (14):

$$\int_0^\infty G(t)\,\mathrm{d}t = m\left(c_\mathrm{f}\int_0^\infty G_\mathrm{s}(t)\,\mathrm{d}t + \int_0^\infty\int_0^\infty G_\mathrm{s}(t')\dot{c}_\mathrm{s}(t-t')\,\mathrm{d}t'\,\mathrm{d}t\right)$$
$$= m\left(c_\mathrm{f} + \int_0^\infty \dot{c}_\mathrm{s}(t')\,\mathrm{d}t'\right) = m(c_\mathrm{f} + c_\mathrm{s}\,(t\to\infty))$$
$$= mc_{p,0} \tag{17}$$

Because of the characteristic behavior of the Fourier transformation the integral of $G(t)$ is related to $g^*(\omega)$:

$$\int_0^\infty G(t)\,\mathrm{d}t = g^*(\omega\to 0) \tag{18}$$

The characteristic impulse response function $g^*(\omega)$ can be measured directly using a stochastic temperature modulation with a wide frequency range. This function includes all the information of the dynamics of the system (sample and instrument). Furthermore $g^*(\omega)$ is the apparent complex heat capacity, which can be calibrated using a complex calibration function, as it is well known from the conventional TMDSC [9,10]. According to Eqs. (17) and (18) the integral of $G(t)$ or the limit of $g^*(\omega\to 0)$ is directly the quasi-static heat capacity $c_{p,0}$. Using this evaluation, no dedicated calibration procedures for $c_{p,0}$ are necessary.

According to Eq. (15) the result of the convolution of the heating rate (input function) and the step response function is the smeared sensible heat flow $\Phi_\mathrm{sens,s}$:

$$\Phi_\mathrm{sens,s}(t) = G(t)\otimes\beta(t) \tag{19}$$

The latent heat flow

$$\Phi_\mathrm{lat}(t) = m\Delta h_\mathrm{r}\dot{\alpha} \tag{20}$$

is the result of the underlying physical or chemical processes. The measured heat flow according to Eq. (15) can be described by the signal flow diagram in Fig. 1. The input signal is the (measured) heating rate given by the constant underlying heating rate β_u and the heating rate β_mod of the stochastic temperature modulation. The system is the DSC instrument including crucibles and sample. This system is characterized by the step response function $G(t)$. The heat flow component related to the heating rate is the smeared sensible heat flow. This component is overlapped by the latent heat flow, which is almost independent of the temperature perturbation. Because of the relatively slow dynamics of this heat flow component and the relatively low underlying heating rate by TMDSC, this component is practically not influenced by smearing due to heat transfer. The measured heat flow is the sum of the smeared sensible heat flow and the latent heat flow. Stochastic temperature modulation and appropriate data processing allows the separation of latent and sensible heat flow, the determination of the quasi-static heat capacity without special calibration procedures, and the measurement of the frequency-dependent apparent complex heat capacity over a wide frequency range. This is the basis of the TOPEM® technology developed by METTLER TOLEDO.

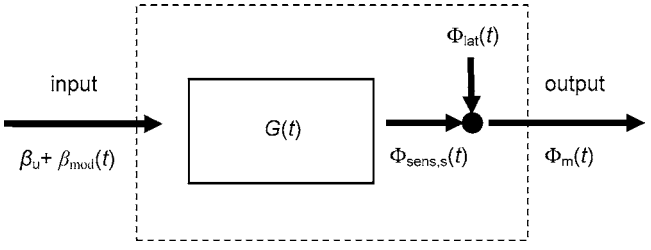

Fig. 1. Schematic of the signal flow in a DSC. β_u is the underlying heating rate and β_mod the additional heating rate due to the modulation function. $\Phi_\mathrm{sens,s}$ is the smeared sensible heat flow, Φ_lat the latent heat flow and Φ_m is the measured heat flow.

3. Experimental and data evaluation

3.1. The experimental approach

Eqs. (15)–(18) yield the fundamental principles of stochastic temperature-modulated DSC as realized in TOPEM® technology. The basic idea involves four main steps:

(i) Selection of a modulation function that includes a broad frequency spectrum. This is a stochastic temperature perturbation.
(ii) Separation of the measured heat flow into two components according to Eq. (17). One component is correlated with the heating rate. This is the smeared sensible heat flow. The other component, which is not correlated with the heating rate, is the latent heat flow component. In accordance with terminology frequently used in TMDSC, this component is the non-reversing heat flow Φ_non.
(iii) The step response function $g^*(\omega)$ is derived by analysis of the correlation between the smeared sensible heat flow component and the heating rate. The quasi-static heat capacity $c_{p,0}$ is determined by Eq. (18). From this property, the reversing heat flow is calculated by multiplication of the underlying heating rate and the sample mass: $\Phi_\mathrm{rev} = mc_{p,0}\beta_\mathrm{u}$. The so-called total heat flow is the sum of the reversing and non-reversing heat flows
(iv) Determination of the complex heat capacity according to Eq. (16) for each selected frequency. For the determination of the calibration function, the data of $c_{p,0}$ outside of the transition can be used.

The names non-reversing and reversing heat flow emphasize that these components are the results of evaluation procedures. The identity $\Phi_\mathrm{non} = \Phi_\mathrm{lat}$ is only valid if the measurement conditions are within the limits of linearity. This means that the temperature step of the stochastic temperature perturbation δT and the underlying heating rate must be sufficiently small. The reversing heat flow becomes the same as the sensible heat flow at the selected underlying heating rate $\Phi_\mathrm{sens}(\beta_\mathrm{u})$ if the related frequency in addition approaches zero. These limitations are not specific to stochastic temperature modulation and have to be taken into account in all TMDSC techniques.

Using stochastic temperature modulation and data processing as realized by TOPEM® the dynamic behavior of the sample can

be analyzed over a wide frequency range in one single measurement. The reversing heat flow signal based on the quasi-static heat capacity and the non-reversing heat flow signal is a direct result of the correlation analysis.

3.2. Temperature program

For stochastic temperature-modulated DSC, a large number of modulation functions and evaluation procedures can be used [28]. The experiments were performed using a METTLER TOLEDO DSC823^e equipped with a FRS5 sensor. The temperature perturbation can be described by Eq. (3): $\delta T(t) = \delta T_0 f_{mod}(t)$. The modulation function $f_{mod}(t)$ is generated as a stochastic series of temperature pulses. (Fig. 2). Δt_p is both the time between the pulses and the pulse width. It is generated by a random number generator between two selected limits, the minimum, Δt_{min}, and the maximum limit, Δt_{max}. The modulation function switches between ± 1.

The lower time limit $\Delta t_{p,min}$ is given by the signal time constant of the instrument including the influence of crucible. This time should be large enough that the sample can respond to the temperature step. Under standard conditions this time $\Delta t_{p,min}$ is set to be 15 s. The maximum time $\Delta t_{p,max}$ is related to the thermal behavior of the sample. If a frequency-dependent heat capacity is to be measured over a wide frequency range, $\Delta t_{p,max}$ should be set to 100 s or larger. In this case a low underlying heating rate should be selected. If a wide frequency range is not important, $\Delta t_{p,max}$ can be set to lower values. The standard value is 30 s.

The maximum temperature perturbation, δT_0, is a parameter that is important to fulfill linearity conditions. The maximum value of δT_0 depends on the thermal event. For example, during a glass transition and cold crystallization, a value of 0.5 K is small enough. However, during a critical phase transition, δT_0 should be in the order of 1 mK.

The program temperature is determined by superimposition of the temperature due to the underlying heating rate and the temperature modulation. A typical measured temperature signal using the default parameters is shown in Fig. 3.

To illustrate the resulting temperature change, a measured temperature curve is shown in Fig. 3. This data is used for further data processing. The frequency spectrum of such a temperature

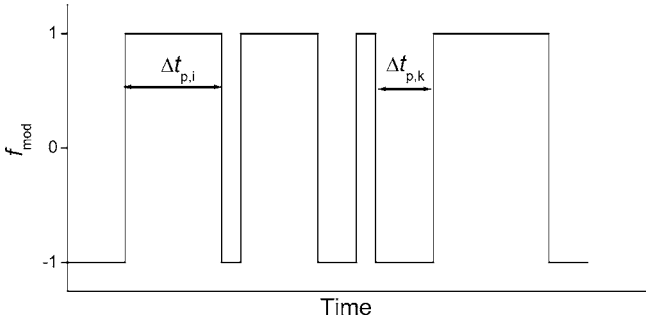

Fig. 2. Segment of a typical modulation function. The pulse time Δt_p at the position i and k are marked.

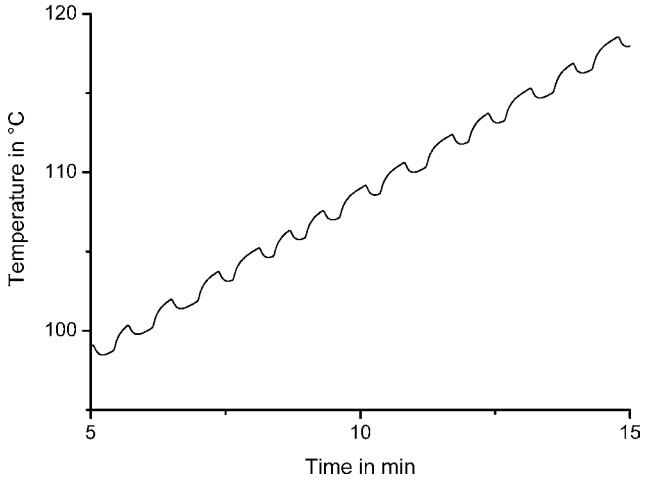

Fig. 3. Part of a typical temperature function.

program is shown in Fig. 4. It is almost constant in the relevant frequency range.

Part of a typical heat flow curve is shown in Fig. 5.

3.3. Data evaluation procedure

The heat flow $\Phi_m(k\Delta t)$ and the temperature $T_m(k\Delta t)$ data are measured using an analog-digital converter ($k = 1, 2, \ldots$). A sampling interval, Δt of 0.1 s was selected. A common transformation for such a discrete function is the z-transformation:

$$\Phi_m(z) = \sum_{i=0}^{\infty} \Phi_m(i\Delta t) z^{-i} \tag{21}$$

To convert the z-transformed function to a discrete Fourier transformed function, z has to be substituted by $e^{j\omega\Delta t}$. In accordance with the Fourier transformation the convolution product becomes a simple algebraic product in the z-space. Consequently the z-transformed measured heat flow is (Eq. (15))

$$\Phi_m(z) = g(z)\beta(z) + \Phi_{lat}(z) = \Phi_{sens,s}(z) + \Phi_{lat}(z) \tag{22}$$

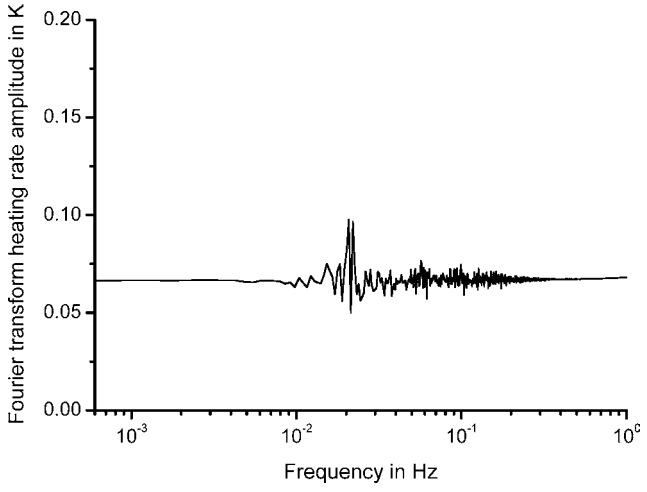

Fig. 4. Spectrum of the heating rate amplitude determined from a 30 min segment of the measured temperature.

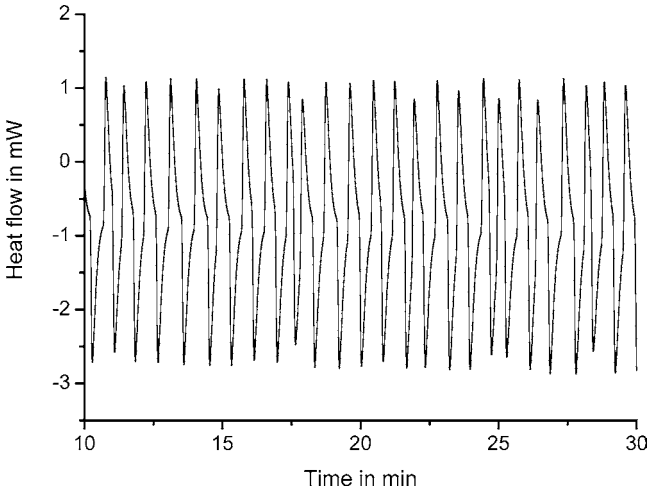

Fig. 5. Segment of a measured heat flow curve.

where $g(z)$ and $\beta(z)$ are the z-transformation of $G(t)$ and $\beta(t)$, respectively. A strategy to find a numerical stable solution is the approach to describe the impulse response function $g(z)$ as a rational multi-parametric function:

$$g(z) = \frac{\sum_{i=0}^{p} b_i\, z^{-i}}{\sum_{i=0}^{q} a_i\, z^{-i}} \tag{23}$$

where b_i and a_i are parameters. The parameter a_0 is usually set to $a_0 = 1$.

Eqs. (22) and (23) are the basis of the data evaluation procedure. The results depend not only on the numerical procedure but also on the quality of the experimental data. This means the experimental parameters must be adequate (low underlying heating rate, small temperature perturbation and large frequency range). If this is not fulfilled, the numerical algorithm produces data that should not be discussed in the framework of thermodynamics. Because of this possibility, in Eq. (22) we substitute the terms sensible and latent heat flow with reversing and non-reversing heat flow [26]. Eq. (22) then becomes

$$\Phi_m(z) = g(z)\beta(z) + \Phi_{non} = \Phi_{rev}(z) + \Phi_{non}(z) \tag{24}$$

For simplification of the following calculations, the non-reversing heat flow is set to be a constant in the time-domain. This is a good practical approximation, but not necessary for our further discussion.

By inserting Eq. (23) in Eq. (24), application of the translation operation of the z-transformation ($\Phi(z)z^{-i} = \Phi((n-i)\Delta t)$ and execution of simple algebraic operations, it follows for the kth data point that

$$\Phi_m(k\Delta t) = \sum_{i=0}^{p} b_i \beta((k-i)\Delta t) - \sum_{i=1}^{q} a_i \Phi_m((k-i)\Delta t) + \Phi_{non} \sum_{i=0}^{q} a_i \tag{25}$$

This equation emphasizes that the actual value of the heat flow is determined by the heat flow signals in the past (between $(t - q\Delta t)$ and $(t - \Delta t)$) and the heating rate between $((t - p\Delta t)$ and t. The related time intervals depend on the dynamic behavior of the sample and the instrument. For example, $p\Delta t$ depends on the time constant of the DSC sensor. The larger the time constant, the larger is p at a given sampling interval Δt.

In the numerical evaluation procedure, Eq. (25) is set up for each data point in the relevant interval. Φ_{non} and the parameters a_i and b_i are determined by solution of the resulting system of linear equations. Such a procedure is related to step (ii) of the TOPEM® procedure described above. The non-reversing heat flow is thus a direct result of the first step of the evaluation procedure. The resulting parameters a_i and b_i describe the frequency-dependent characteristic function $g^*(\omega)$.

To realize step (iii) of the TOPEM® procedure (determination of the quasi-static heat capacity, $c_{p,0}$ and the reversing heat flow) we have to determine $g^*(\omega \to 0)$.The non-reversing heat flow is given by

$$\Phi_{non} = m c_{p,0} \beta_u \tag{26}$$

The total heat flow is the sum of both independently determined heat flow components

$$\Phi_{tot} = \Phi_{rev} + \Phi_{non} \tag{27}$$

As mentioned above, the non-reversing heat flow determined by the TOPEM® procedure is independent of selected frequencies. It is related to quasi-static conditions. Furthermore, the non-reversing heat flow is directly determined. Consequently, these properties can be linked to the thermodynamic properties like sensible and latent heat flow. If the measurement is performed under almost linear and stationary conditions, agreement between the reversing and sensible heat flow and between the non-reversing and latent heat flow improves. Such conditions can be achieved with small temperature perturbation and sufficiently low underlying heating rates.

In step (iv) of the TOPEM® procedure, the complex frequency-dependent heat capacity $c_p^*(\omega)$ is determined at different selected frequencies. According to Eq. (16) the apparent (non-calibrated) complex heat capacity, $c_{p,a}^*(\omega)$, can be directly determined using the parameter set. One way to determine the calibration function $g_s^*(\omega)$ is a comparison of the absolute value of the apparent complex heat capacity at each selected frequency ω_0 with the quasi-static heat capacity. Outside a thermal event region, $c_p^*(\omega_0)| = c_{p,0}$ and $\varphi = 0$. The phase φ is related to the ratio of the imaginary and real part of the heat capacity: $\varphi = \arctan(c''/c')$. Consequently, it follows that in such a region of the curve

$$|g_s^*(\omega_0)| = \frac{c_{p,0}}{|c_{p,a}^*(\omega_0)|} \quad \text{and} \quad \varphi = 0 \tag{28}$$

Procedures to calibrate inside the transition region are described elsewhere [9,33–35].

4. Results and discussion

4.1. Frequency dependence of the glass transition

The glass transition of a technical polystyrene (PS) ($M_w = 350{,}000$ and $M_n = 170{,}000$) was measured using a

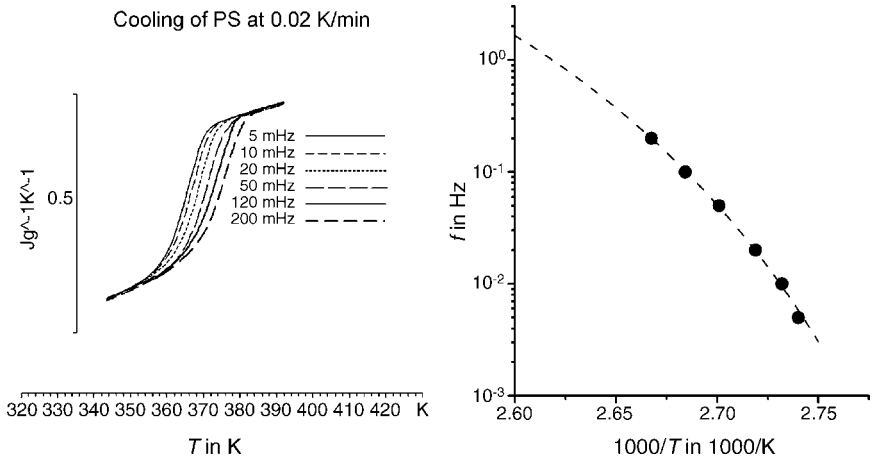

Fig. 6. The real part of the complex heat capacity c'_p at different frequencies in the glass transition region of polystyrene (right) and the resulting activation diagram (left). The dashed line represents a fit using the Vogel-Fulcher equation.

underlying heating rate of 0.02 K/min. The maximum temperature perturbation of the modulation function was $\delta T_0 = 0.5$ K (Fig. 6). The times between the pulses were set to be between $\Delta t_{p,min} = 1$ s and $\Delta t_{p,max} = 100$ s. The heat capacity change in the glass transition region was evaluated at frequencies between 5 mHz and 200 mHz. This frequency range could be swept in a single measurement. The glass transition temperature T_g was determined for each frequency as the temperature of the half step height. T_g increases with increasing frequency. In the left part of Fig. 6 the data are plotted in an activation diagram ($\log f$ versus $1/T$). The measured points are fitted using the Vogel-Fulcher equation

$$f = A \exp\left(-\frac{B}{T - T_v}\right) \quad (29)$$

where A is the pre-exponential factor, B the curvature parameter and T_v is the Vogel temperature [23]. The parameters for the fit in Fig. 6 are $A = 2 \times 10^6\ s^{-1}$, $B = 500$, $T_v = 334$ K.

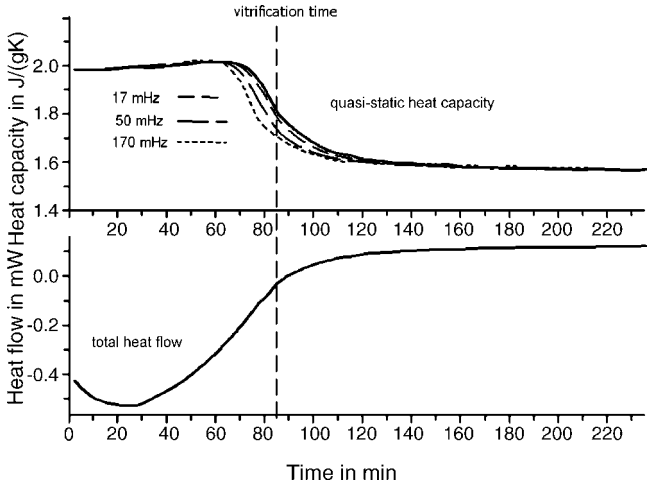

Fig. 7. Heat capacity curves (upper) and the total heat flow curve (lower) measured during isothermal curing of the system DGEBA-DDM at 80 °C.

4.2. Isothermal curing of a thermoset

A thermoset consisting stoichoimetric amounts of diglycidylether of bisphenol A (DGEBA) and diaminodiphenyl methane (DDM) was cured isothermally at 80 °C (Fig. 7). The total heat flow curve shows the course of the exothermic reaction (lower part in Fig. 7). At the same time, the quasi-static heat capacity curve can also be determined (Fig. 7, upper part). As the reaction proceeds, $c_{p,0}$ first increases linearly and then decreases in a step. This step is a result of vitrification that occurs in the course of the reaction. After vitrification, diffusion is hindered. This causes the reaction rate to slow down dramatically so that the reaction almost stops. The vitrification time of 86.5 min (determined from $c_{p,0}$) is therefore an important value for characterizing the curing reaction.

Since vitrification is in fact a chemically induced glass transition [36], the c'_p–curing time curve is also frequency dependent. The multi-frequency evaluation shows that at higher frequency the step is shifted to shorter times. One advantage of this evaluation is that the curves for different frequencies can be determined

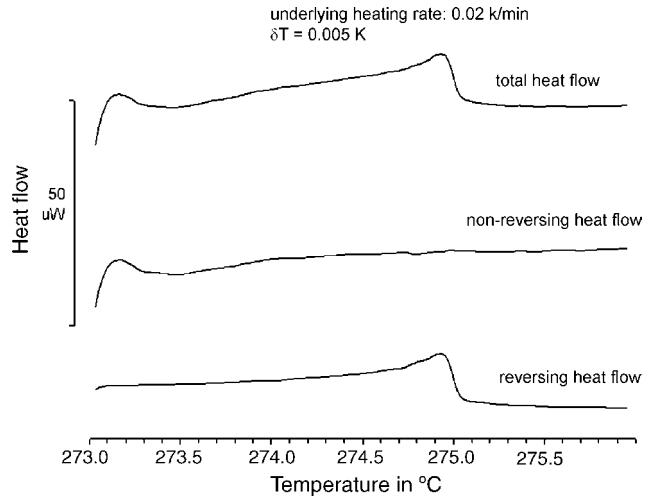

Fig. 8. Quasi-static heat capacity and the total, reversing and non-reversing heat flow curves of the solid–solid transition of sodium nitrate.

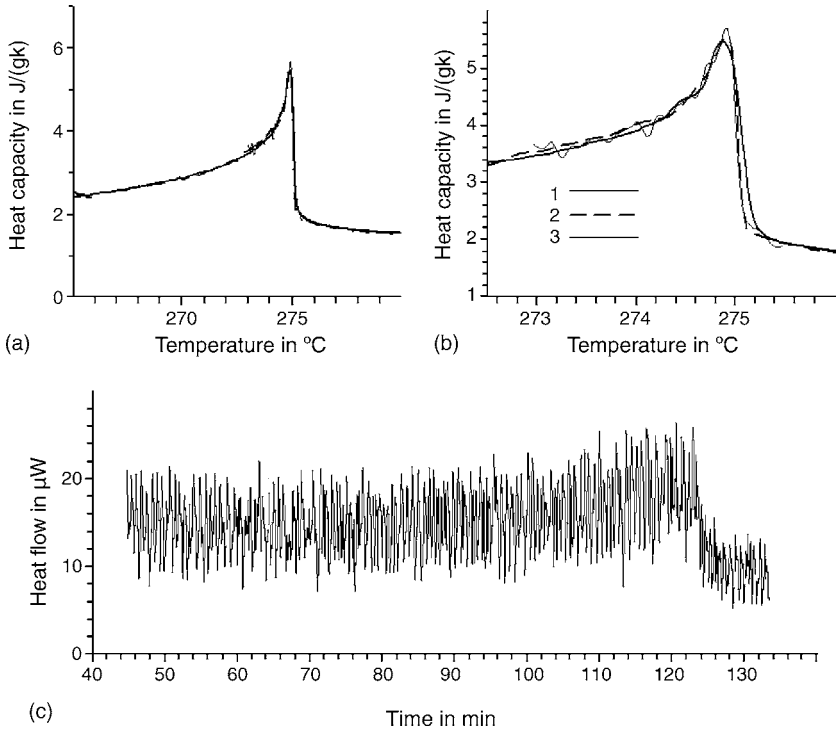

Fig. 9. (a) The heat capacity curves of $NaNO_3$ in the temperature range 265 °C and 280 °C, measured at different temperature programs (curve 1: β_u = 0.125 K/min, δT_0 = 0.1 K; curve 2: β_u = 0.125 K/min, δT_0 = 0.01 K; curve 3: β_u = 0.02 K/min, δT_0 = 0.001 K). (b) Scale expansion of diagram (a) in the temperature range between 272.5 °C and 276 °C. (c) Measured heat flow curve at β_u = 0.02 K/min and δT_0 = 0.001 K.

from a single measurement of the same sample, so that differences in the composition of different samples are not a source of error.

4.3. Solid–solid transition of sodium nitrate

Sodium nitrate shows a second order phase transition around 275 °C [37]. In the phase transition of sodium nitrate the heat capacity first increases with increasing temperature and then suddenly decreases within 100 mK at the critical temperature. To gain information about the physical nature of such transitions, measurements have to be performed at very low heating rates (20 mK/min) and very small temperature modulations (δT_0 = 5 mK). As shown in Fig. 8, the non-reversing heat flow curve indicates that the transition occurs without the release of excess heat. This behavior is expected for a second-order phase transition. For this measurement the reversing heat flow is the sensible heat flow at the underlying heating rate. The non-reversing heat flow becomes identical to the latent heat. The separation between latent and sensible heat flow is clearly shown in Fig. 8.

The repeatability even at very low amplitudes is shown in Fig. 9. This figure shows the heat capacity curves measured under different conditions. In the upper diagram on the right the abscissa scale has been expanded to show the differences for different settings of δT_0. The diagram on the left gives a general overview. The underlying heating rates used were 0.125 K/min and 0.01 K/min, respectively. The step height of the temperature perturbation δT_0 was selected to be 0.1 K, 0.01 K and 0.001 K. All $c_{p,0}$- curves show a good agreement in the absolute heat capacity. Only the curve with the largest δT_0 is slightly broader in the region after the sharp decrease in heat capacity above the critical temperature of about 275 °C. This is due to non-linear conditions in the measurement. To improve the quality of the experimental data, δT_0 should be reduced. The best results are obtained at δT_0 = 0.01 K. Even for the very small temperature perturbation at δT_0 = 1 mK, the related curve shows very good agreement with the curve measured with δT_0 = 0.01 K. Only the noise is somewhat higher at this extremly small temperature modulation. To get an impression of the curve analyzed, the raw heat flow curve measured at β_u = 0.02 K/min and δT_0 = 1 mK is also plotted in Fig. 9. The peak-to-peak distance of the stochastic heat flow signal is as low as 10 µW.

5. Conclusions

Information of thermal relaxation behavior can be obtained from temperature-modulated DSC using a stochastic temperature modulation technique. Based on the general theory of temperature-modulated calorimetry the data evaluation is described. By analyzing the correlation between the heating rate and heat flow, information on the dynamic behavior of the sample and the instrument are determined. This analysis yields the quasi-static heat capacity $c_{p,0}$ and the frequency-dependent complex heat capacity $c_p^*(\omega)$ without the need for additional calibration procedures. $c_p^*(\omega)$ can be determined over a wide frequency range. A second result is the non-reversing heat flow Φ_{non}. This is the non-correlated heat flow component.

The reversing heat flow is calculated from the quasi-static heat capacity. All these quantities and their frequency dependence can be determined in one single measurement.

At sufficiently low underlying heating rates and small temperature perturbations, the resulting reversing and non-reversing heat flows become identical to the sensible and latent heat flow components for the underlying heating rate.

The concept of stochastic temperature-modulated DSC has been recently realized in TOPEM® by METTLER TOLEDO.

References

[1] P. Claudy, J.C. Commercon, J.M. Letoffe, Thermochim. Acta 128 (1988) 251.
[2] M. Reading, D. Elliott, V.L. Hill, J. Therm. Anal. 40 (1993) 949.
[3] J.E.K. Schawe, J. Therm. Anal. 47 (1996) 475.
[4] M. Cassettari, G. Salvetti, E. Tombari, S. Veronesi, G.P. Johari, Il Nuovo Cimento 14D (1992) 763.
[5] G. van Assche, A. van Himelrijck, H. Rahier, B. van Mele, Thermochim. Acta 304/305 (1997) 317.
[6] I. Alig, W. Jenninger, J.E.K. Schawe, Thermochim. Acta 330 (1999) 167.
[7] M. Schubnell, J.E.K. Schawe, Int. J. Pharm. 217 (2001) 173.
[8] J.E.K. Schawe, U. Hess, J. Therm. Anal. Cal. 68 (2002) 741.
[9] J.E.K. Schawe, W. Winter, Thermochim. Acta 298 (1997) 9.
[10] I. Moon, R. Androsch, B. Wunderlich, Thermochim. Acta 357–358 (2000) 285.
[11] N.O. Birge, P.K. Dixon, N. Menon, Thermochim. Acta 304–305 (1997) 51.
[12] E. Donth, J. Korus, E. Hempel, M. Beiner, Thermochim. Acta 304–305 (1997) 239.
[13] J.E.K. Schawe, E. Bergmann, Thermochim. Acta 304–305 (1997) 179.
[14] J.E.K. Schawe, J. Polym. Sci. B: Polym. Phys. 36 (1998) 2165.
[15] H. Huth, M. Beiner, S. Weyer, M. Merzlyakov, C. Schick, E. Donth, Thermochim. Acta 377 (2001) 113.
[16] J.E.K. Schawe, G.R. Strobl, Polymer 39 (1998) 3745.
[17] S.C. Mraw, D.F. Naas, J. Chem. Thermodyn. 11 (1979) 567.
[18] W.F. Hemminger, H.K. Cammenga, Methoden der Thermischen Analyse, Springer-Verlag, Berlin, 1989, p. 260 ff.
[19] R. Riesen, G. Widmann, R. Truttmann, Themochim. Acta 272 (1996) 27.
[20] H. Gobrecht, K. Hamann, G. Willers, J. Phys. E: Sci. Instrum. 4 (1971) 21.
[21] U. Jörimann, G. Widmann, R. Riesen, J. Therm. Anal. Cal. 56 (1999) 639.
[22] J.E.K. Schawe, Thermochim. Acta 271 (1996) 127.
[23] A. Hensel, J. Dobbertin, J.E.K. Schawe, A. Boller, C. Schick, J. Therm. Anal. 46 (1996) 935.
[24] B. Wunderlich, R. Androsch, M. Pyda, Y.K. Kwon, Thermochim. Acta 348 (2000) 181.
[25] M. Merzlyakov, C. Schick, Thermochim. Acta 380 (2001) 5.
[26] M. Reading, Trends Polym. Sci. 1 (1993) 248.
[27] J.E.K. Schawe, Thermochim. Acta 260 (1995) 1.
[28] J. Schawe, I. Alig, D. Lellinger, EP 1091208 (2001);
J. Schawe, I. Alig, D. Lellinger, US Patent 6,551,835 (2001).
[29] J.E.K. Schawe, S. Thobald, J. Non-Cryst. Solids 235-237 (1998) 496.
[30] C. Schick, M. Merzlyakov, A. Hensel, J. Chem. Phys. 111 (1999) 2695.
[31] G.W.H. Höhne, J.E.K. Schawe, Thermochim. Acta 229 (1993) 27.
[32] J.E.K. Schawe, C. Schick, G.W.H. Höhne, Thermochim. Acta 244 (1994) 49.
[33] A. Toda, M. Hikosaka, Thermochim. Acta 436 (2005) 15.
[34] S. Weyer, A. Hensel, C. Schick, Thermochim. Acta 304–305 (1997) 267.
[35] Z. Jiang, C.T. Imrie, J.M. Hutchinson, Thermochim. Acta 315 (1998) 1.
[36] J.E.K. Schawe, I. Alig, Colloid Polym. Sci. 279 (2001) 1169.
[37] G.L. Janz, F.J. Kelly, J.L. Pérano, J. Chem. Eng. Data 9 (1964) 133.